Electrical and thermal transport properties of the kagome metals ATi$_3$Bi$_5$ (A = Rb, Cs)

Xintong Chen,[1,*] Xiangqi Liu,[2,*] Wei Xia,[2,3] Xinrun Mi,[1] Luyao Zhong,[1] Kunya Yang,[1] Long Zhang,[1] Yuhan Gan,[1] Yan Liu,[4] Guiwen Wang,[4] Aifeng Wang,[1] Yisheng Chai,[1] Junying Shen,[5,6] Xiaolong Yang,[1,†] Yanfeng Guo,[2,3,‡] and Mingquan He[1,§]

[1]*Low Temperature Physics Laboratory, College of Physics & Center of Quantum Materials and Devices, Chongqing University, Chongqing 401331, China*

[2]*School of Physical Science and Technology, ShanghaiTech University, Shanghai 201210, China*

[3]*ShanghaiTech Laboratory for Topological Physics, Shanghai 201210, China*

[4]*Analytical and Testing Center, Chongqing University, Chongqing 401331, China*

[5]*Institute of High Energy Physics, Chinese Academy of Sciences (CAS), Beijing 100049, China*

[6]*Spallation Neutron Source Science Center, Dongguan 523803, China*

(Received 7 March 2023; revised 25 April 2023; accepted 26 April 2023; published 10 May 2023)

We report electrical and thermal transport properties of single-crystalline kagome metals ATi$_3$Bi$_5$ (A = Rb, Cs). Different from the structrually similar kagome superconductors AV$_3$Sb$_5$, no charge density wave instabilities are found in ATi$_3$Bi$_5$. At low temperatures below 5 K, signatures of superconductivity appear in ATi$_3$Bi$_5$ as seen in magnetization measurements. However, bulk superconductivity is not evidenced by specific heat results. Similar to AV$_3$Sb$_5$, ATi$_3$Bi$_5$ show a nonlinear magnetic field dependence of the Hall effect below about 70 K, pointing to a multiband nature. Unlike AV$_3$Sb$_5$ in which phonons and electron-phonon coupling play important roles in thermal transport, the thermal conductivity in ATi$_3$Bi$_5$ is dominated by electronic contributions. Moreover, our calculated electronic structures of ATi$_3$Bi$_5$ suggest that van Hove singularities are sitting well above the Fermi energy. Compared with AV$_3$Sb$_5$, the absence of charge orders in ATi$_3$Bi$_5$ is closely associated with minor contributions from electron-phonon coupling and/or van Hove singularities.

DOI: 10.1103/PhysRevB.107.174510

I. INTRODUCTION

The kagome lattice is a two-dimensional structure, which is made up of corner-sharing triangles [1]. Interestingly, the electronic structure of the kagome lattice hosts Dirac cones, van Hove singularities, and a flat band [2]. Various quantum phases of matter including quantum spin liquids, topological orders, and unconventional superconductivity could arise from the kagome lattice by tuning the electron filling [3–8]. Materials containing a kagome lattice are thus prominent platforms to study the interplay of lattice, spin, and charge degrees of freedom. Among various kagome materials, the recently discovered kagome metals AV$_3$Sb$_5$ (A = K, Rb, Cs) are of particular interest [9–12]. In AV$_3$Sb$_5$, V atoms form an ideal kagome structure at room temperature, giving rise to two van Hove singularities around the M point, Dirac-like and $\mathbb{Z}_2$ topological bands near the Fermi level [13–17]. More interestingly, a chiral charge density wave (CDW) associated with a giant anomalous Hall effect and time-reversal symmetry breaking emerges below $T_{CDW} \sim$ 80–100 K [18–35]. At low temperatures below $T_c \sim$ 0.9–2.5 K, a superconducting phase arises and competes with the CDW phase [36–46]. Extensive studies are undergoing to explore the origins of the unusual charge orders and superconductivity.

The discoveries of kagome metals AV$_3$Sb$_5$ motivated much research effort to search for structurally similar materials. Quite a few vanadium-based kagome compounds, such as AV$_6$Sb$_6$, AV$_8$Sb$_{12}$, V$_6$Sb$_4$, and RV$_6$Sn$_6$, have been reported experimentally [47–52]. In addition to theses systems, Yi *et al.* [53] and Jiang *et al.* [54] predicted various thermodynamically stable AV$_3$Sb$_5$-like kagome materials based on first-principles calculations. Notably, among the theoretically predicted AV$_3$Sb$_5$-like compounds, titanium-based kagome metals ATi$_3$Bi$_5$ (A = Rb, Cs) have been experimentally synthesized lately [55–60]. Below 4 K, resistivity measurements on RbTi$_3$Bi$_5$ and CsTi$_3$Bi$_5$ revealed signatures of superconductivity, which were attributed to RbBi$_2$/CsBi$_2$ impurities by Werhahn *et al.* [55]. On the other hand, recent studies performed by Yang *et al.* favor a bulk nature of superconductivity in CsTi$_3$Bi$_5$ [56,57]. Moreover, $\mathbb{Z}_2$ topological characters and electronic nematicity have been suggested in CsTi$_3$Bi$_5$ [56–58]. Near the Fermi energy, flat bands and Dirac nodal lines have been identified in RbTi$_3$Bi$_5$ [58,59]. Using an external stimulus, such as biaxial strain, van Hove singularities could be tuned to the Fermi level, which may lead to CDW and/or superconductivity [60]. It appears that ATi$_3$Bi$_5$ is a prominent system to explore nematic order and topological properties. Importantly, ATi$_3$Bi$_5$ does not show charge density wave instabilities [55–60]. Therefore, comparing the similarities and differences between ATi$_3$Bi$_5$ and AV$_3$Sb$_5$ can provide crucial clues for unraveling the mechanisms of CDW in AV$_3$Sb$_5$.

In this paper, we present electrical and thermal transport measurements on ATi$_3$Bi$_5$ (A = Rb, Cs) single crystals.

*These authors contributed equally to this work.
†yangxl@cqu.edu.cn
‡guoyf@shanghaitech.edu.cn
§mingquan.he@cqu.edu.cn

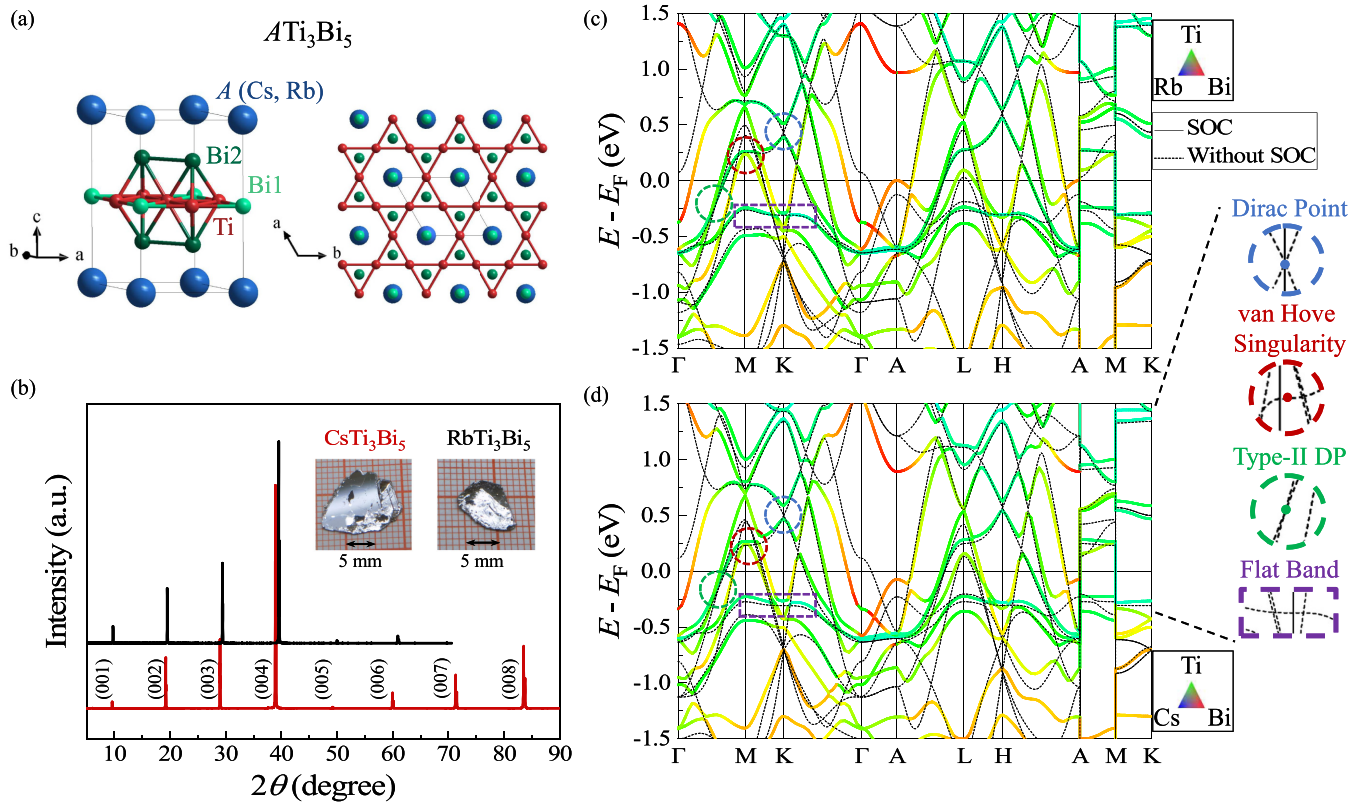

FIG. 1. (a) Side (left panel) and top (right panel) views of the crystal structure of ATi_3Bi_5 (space group: $P6/mmm$). The Ti atoms form a kagome lattice in the Ti-Bi layer with one type of Bi atoms (Bi1) sitting in the center of kagome hexagons. The other type of Bi atoms (Bi2) locate above and below the Ti-Bi1 layer, forming a honeycomb pattern. (b) X-ray diffraction patterns of $RbTi_3Bi_5$ (black curve) and $CsTi_3Bi_5$ (red curve) single crystals. The $(00L)$ peaks can be nicely identified. The inset in (b) shows photographs of typical ATi_3Bi_5 samples. (c) and (d) Calculated electronic band structures of $RbTi_3Bi_5$ and $CsTi_3Bi_5$ with (solid lines) and without (dashed lines) considering spin-orbit coupling.

No bulk superconductivity is found in our ATi_3Bi_5 samples. Similar to AV_3Sb_5, the multiband electronic structure plays important roles in the electrical transport of ATi_3Bi_5. On the other hand, minor contributions from phonons and electron-phonon coupling are seen in the thermal transport of ATi_3Bi_5, which is different from that in AV_3Sb_5. One more difference between ATi_3Bi_5 and AV_3Sb_5 is that the separations between van Hove singularities and the Fermi level in ATi_3Bi_5 are much larger than those in AV_3Sb_5. These differences may hold the key for the absence of CDW in ATi_3Bi_5.

II. EXPERIMENTAL METHOD

Single crystals of ATi_3Bi_5 samples were prepared by a self-flux method [59]. Shiny crystals with in-plane sizes up to centimeters were obtained, as shown in the inset of Fig. 1(b). Magnetization and heat capacity measurements were carried out in a physical property measurement system (PPMS, Quantum Design Dynacool 9 T) using a vibrating sample magnetometer and relaxation method, respectively. The Seebeck effect and thermal conductivity were performed using the steady state method in PPMS on a home-made insert equipped with one heater and two thermometers. The electrical transport measurements were recorded using the Hall bar geometry. The ATi_3Bi_5 crystals degrade easily when exposed to ambient atmosphere. To prevent sample degradation, all experimental preparations were conducted in a glove box filled with argon.

Density functional theory (DFT) [61] calculations were performed to calculate the electronic band structure of $CsTi_3Bi_5$ and $RbTi_3Bi_5$ using the Vienna *ab initio* simulation package (VASP) [62,63] with the projector augmented-wave method (PAW) [64,65]. The Perdew-Burke-Ernzerhof (PBE) parametrization of the generalized gradient approximation (GGA) was employed to treat the exchange-correlation energy functional [66]. A plane-wave cutoff energy of 520 eV was used, and a convergence threshold of 10^{-7} eV was adopted for each self-consistent electronic step. Cell parameters and internal atomic positions were fully relaxed with a k mesh of $23\times23\times11$ until the maximum force on each atom was less than 10^{-3} eV Å^{-1}. The optimized lattice constants are in good agreement with experiments [55–57]. To obtain the precise band structure and corresponding Fermi energy, a $23\times23\times11$ Γ-centered k mesh was adopted based on an equilibrium structure.

III. RESULTS AND DISCUSSION

The crystal structure of ATi_3Bi_5 is similar to that of AV_3Sb_5, as shown in Fig. 1(a). The Ti-Bi layers are sandwiched by the alkali A layers, forming a layered structure within the $P6/mmm$ space group. The key element is the

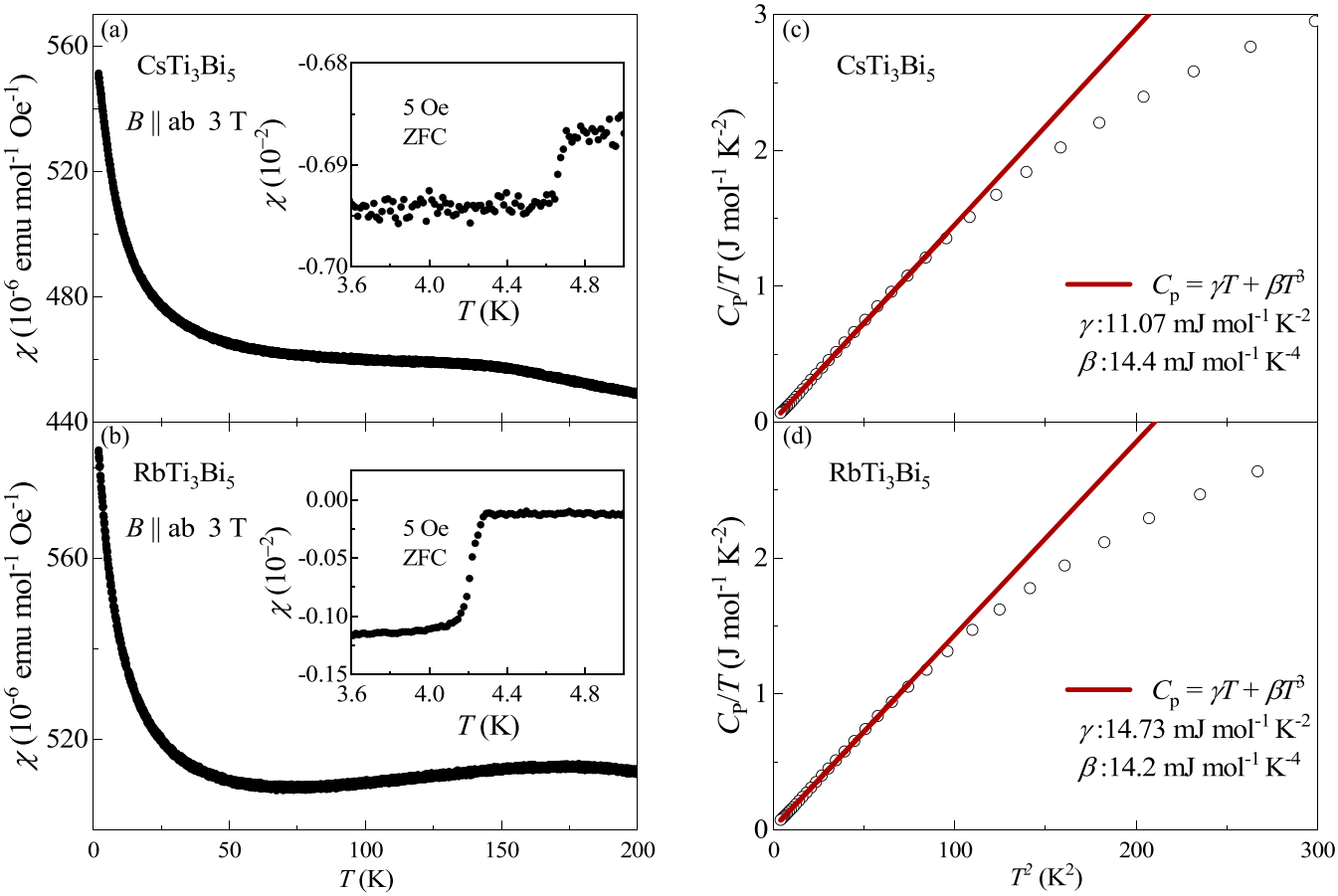

FIG. 2. (a) and (b) Temperature dependence of magnetization $M(T)$ for $CsTi_3Bi_5$ and $RbTi_3Bi_5$ samples. Insets in (a) and (b) show low-temperature zero-field-cooling (ZFC) measurements. (c) and (d) Low-temperature specific heat C_p. The solid red lines in (c) and (d) are theoretical fittings in the form of $C_p/T = \gamma + \beta T^2$.

kagome net formed by Ti atoms, as seen in the right panel of Fig. 1(a). There are two types of Bi atoms with different coordination. The Bi1 atoms are located at the center of Ti kagome hexagons. The Bi2 atoms form a honeycomb pattern, which sits above and below the kagome lattice. The alkali atoms appear in a triangular form. In Fig. 1(b), the x-ray diffraction patterns of typical $RbTi_3Bi_5$ and $CsTi_3Bi_5$ single crystals are presented. The $(00L)$ peaks are clearly seen in both crystals, suggesting the high quality of these samples. The lattice parameters of $RbTi_3Bi_5$ and $CsTi_3Bi_5$ are found to be $a = 5.8248$ Å, $c = 9.2498$ Å and $a = 5.8188$ Å, $c = 9.1507$ Å, respectively, agreeing well with earlier reports [55–57]. Figures 1(c) and 1(d) show the calculated electronic band structures of $RbTi_3Bi_5$ and $CsTi_3Bi_5$. These two isostructural compounds basically show similar electronic band structures with slight differences in details. Despite interruptions introduced by the sizable spin-orbit coupling of the heavy Bi atoms, the featured Dirac points (DPs), van Hove singularities (vHs), and flat bands of the kagome lattice are preserved. These features have been experimentally identified in angle-resolved photoemission spectroscopy measurements [57–59]. Similar to AV_3Sb_5, multiple bands mainly consisting of Ti $3d$ and Bi p_z orbitals cross the Fermi level. There are three electron pockets around the zone center Γ point, and two hole pockets near the zone boundary [58,59]. The multiband nature plays important roles in transport behavior (see Fig. 4). Compared with the V($3d^3$) states in AV_3Sb_5, the Ti($3d^2$) orbitals offer less electrons and lower the Fermi energy (E_F). As a result, the van Hove singularities locating at the M point are pushed well above E_F, while the flat bands come close to E_F. In AV_3Sb_5, it has been suggested that the Fermi-surface nesting promoted by van Hove singularities is responsible for the CDW instabilities [15,18,67–69]. The invisibility of van Hove singularities near E_F may account for the absence of CDW in ATi_3Bi_5.

Figure 2 presents the thermodynamic properties of $CsTi_3Bi_5$ and $RbTi_3Bi_5$. Unlike AV_3Sb_5, the ATi_3Bi_5 family is rather robust against charge density wave instability. As shown in Figs. 2(a) and 2(b), the temperature-dependent magnetization of both compounds shows typical paramagnetic behaviors. No signatures of long-range magnetic orders or charge orders are seen, as also found in previous reports [55–57,59,60]. At low temperatures, traces of the Meissner effect are found below 4.8 and 4.3 K in $CsTi_3Bi_5$ and $RbTi_3Bi_5$, respectively [see the insets in Figs. 2(a) and 2(b)], indicating the possible emergence of superconductivity. The diamagnetic signal is, however, extremely weak. At 2 K, the superconducting volume fraction is less than 1% in an external

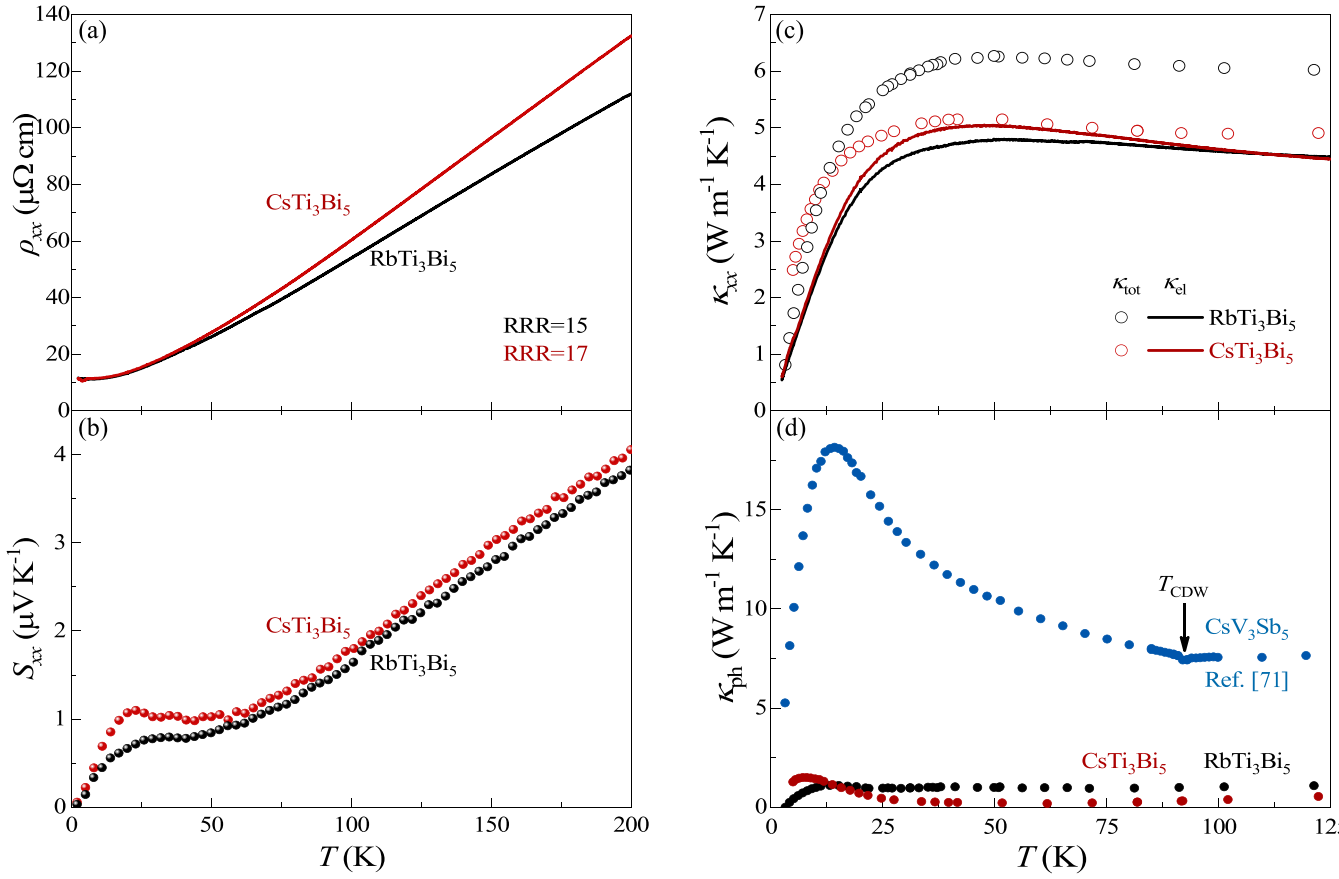

FIG. 3. (a)–(c) Temperature dependence of the longitudinal electrical resistivity (ρ_{xx}), Seebeck effect (S_{xx}), and thermal conductivity (κ_{xx}) of $CsTi_3Bi_5$ and $RbTi_3Bi_5$ crystals. Circular points in (c) represent the total thermal conductivity (κ_{tot}). Solid lines in (c) are calculated electronic thermal conductivity (κ_{el}) according to the Wiedemann-Franz law. (d) Comparison of phonon thermal conductivity (κ_{ph}) in $CsTi_3Bi_5$, $RbTi_3Bi_5$, and CsV_3Sb_5 [71].

magnetic field of 5 Oe. It is likely that the observed weak Meissner signals originate from $CsBi_2$ and $RbBi_2$ impurities, which become superconducting below 4.65 and 4.21 K, respectively [55,70]. As seen in Figs. 2(e) and 2(f), no evidence of a superconducting transition can be identified in the specific heat. This further suggests that bulk superconductivity is absent in samples studied here. By analyzing the low-temperature specific heat according to $C_p = \gamma T + \beta T^3$, the electronic specific heat (Sommerfeld) coefficients γ are estimated to be 11.1(2) and 14.7(3) mJ mol^{-1} K^{-2} for $CsTi_3Bi_5$ and $RbTi_3Bi_5$, respectively. The phonon specific heat coefficients β read 14.4(3) and 14.2(3) mJ mol^{-1} K^{-4} for $CsTi_3Bi_5$ and $RbTi_3Bi_5$, respectively. The Debye temperature Θ_D can be evaluated accordingly following $\beta = 12\pi^4 NR/5\Theta_D^3$ with N and R being the number of atoms per unit cell and the ideal gas constant. It is found that $\Theta_D = 106.63$ and 107.13 K for $CsTi_3Bi_5$ and $RbTi_3Bi_5$, respectively.

The in-plane resistivity (ρ_{xx}) of $CsTi_3Bi_5$ and $RbTi_3Bi_5$ samples measured in zero magnetic field is presented in Fig. 3(a). Both compounds show metallic behaviors. The residual resistivity ratios RRR $= \rho_{xx}(300\ \mathrm{K})/\rho_{xx}(2\ \mathrm{K})$ are 17 and 15 for $CsTi_3Bi_5$ and $RbTi_3Bi_5$ samples, respectively. The thermoelectric Seebeck (S_{xx}) properties are shown in Fig. 3(b). Positive values of S_{xx} are found all the way from room temperature down to 2 K in both samples, implying the dominant roles played by holelike carriers. In AV_3Sb_5, on the other hand, electronlike and holelike excitations compete with each other, leading to sign changes in the Seebeck signal and Hall coefficient at low temperatures [28,29]. Compared with AV_3Sb_5, the Fermi levels of ATi_3Bi_5 shift downwards significantly [see Fig. 1(d)]. As a result, the electron pockets centering at the zone center are reduced, while the hole pockets near the zone boundaries are enlarged. Therefore, it is not unexpected that holelike carriers play major roles in ATi_3Bi_5.

The thermal transport properties of ATi_3Bi_5 are also rather different from those in AV_3Sb_5. As displayed in Fig. 3(c), the total longitudinal thermal conductivity κ_{tot} of $CsTi_3Bi_5$ and $RbTi_3Bi_5$ is dominated by electronic contributions (κ_{el}). The electronic thermal conductivity is estimated from the Wiedemann-Franz law via $\kappa_{el}(T) = \sigma L_0 T$, where σ and L_0 are the electronic conductivity and the Lorenz number. Figure 3(d) compares the phononic thermal conductivity $\kappa_{ph} = \kappa_{tot} - \kappa_{el}$ of $CsTi_3Bi_5$, $RbTi_3Bi_5$, and CsV_3Sb_5. Clearly, κ_{ph} of CsV_3Sb_5 is one order of magnitude larger than that in ATi_3Bi_5. In the charge ordered state below T_{CDW}, κ_{ph} of CsV_3Sb_5 shows typical behaviors of phononic heat transport. Above T_{CDW}, sizable charge fluctuations and electron-phonon coupling lead to glasslike thermal conductivity which increases linearly with warming [71]. In ATi_3Bi_5, κ_{ph} depends weakly on temperature and κ_{el} dominates in heat conduction.

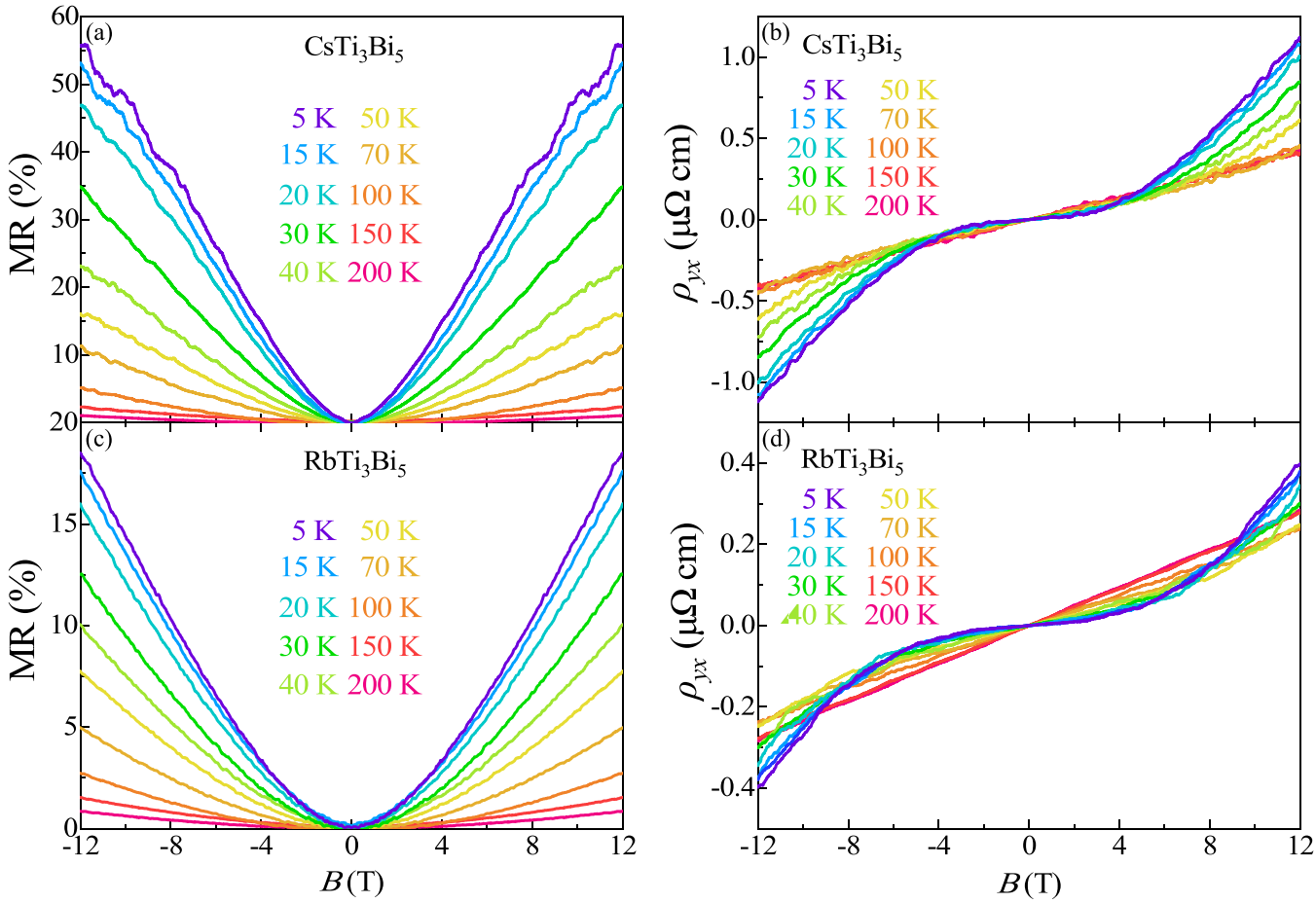

FIG. 4. (a), (c) and (b), (d) Magnetoresistance (MR) and Hall resistivity (ρ_{yx}) of $CsTi_3Bi_5$ and $RbTi_3Bi_5$ recorded at selective temperatures. Nonlinear $\rho_{yx}(B)$ curves appear below 70 K in both materials.

The subdominant roles played by phonons and electron-phonon coupling in ATi_3Bi_5 may also represent important factors for the absence of charge orders.

In Fig. 4, we present the isothermal magnetoresistance (MR) and Hall resistivity (ρ_{yx}) of ATi_3Bi_5. In both materials, positive MR starts to develop below 200 K and becomes more apparent at low temperatures. Large MR $= [\rho_{xx}(B) - \rho_{xx}(0)]/\rho_{xx}(0)$ reaching 55% in 12 T at 5 K is found in $CsTi_3Bi_5$. In $RbTi_3Bi_5$, lower MR values less than 20% are observed at the same conditions. Weak signatures of quantum oscillations are also seen in $CsTi_3Bi_5$ at low temperatures and in high magnetic fields. In both materials above 70 K, the Hall resistivity depends linearly on magnetic field with positive slopes. This implies that the electrical transport is dominated by a single hole band at high temperatures. Further cooling below 70 K, $\rho_{yx}(B)$ becomes nonlinear, pointing to multiband transport. Unlike AV_3Sb_5, no sign changes are found in the temperature-dependent Hall coefficient of ATi_3Bi_5, in accordance with the Seebeck results. Notably, below 20 K, $\rho_{yx}(B)$ shows an S-shaped appearance, which is reminiscent of the anomalous Hall effect found in the CDW phase of AV_3Sb_5 [21,22]. The nontrivial electronic structures near E_F, such as Dirac nodal lines, may produce an anomalous Hall effect. On the other hand, multiband transport can also give rise to such curvatures in $\rho_{yx}(B)$. Considering the multiband nature of ATi_3Bi_5, we use a two-band picture to describe the Hall conductivity,

$$\sigma_{xy}(B) = \frac{-n_e e\mu_e^2 B}{1+\mu_e^2 B^2} + \frac{n_h e\mu_h^2 B}{1+\mu_h^2 B^2}, \tag{1}$$

where $n_{e(h)}$, $\mu_{e(h)}$ are the carrier density and mobility of the corresponding electron (hole) pocket. The experimental Hall conductivity was evaluated from the resistivity data using $\sigma_{xy} = -\rho_{yx}/(\rho_{xx}^2 + \rho_{yx}^2)$. In the two-band fitting process, the constraint for longitudinal electrical conductivity (σ_{xx}) in zero magnetic field was also applied, i.e., $\sigma_{xx}(B=0) = n_e e\mu_e + n_h e\mu_h$. As displayed in Figs. 5(a) and 5(b), the two-band approximation well describes the sublinear Hall conductivity $\sigma_{xy}(B)$ curves below 70 K. It is very likely that the nonlinear magnetic field dependence of the Hall effect observed in ATi_3Bi_5 originates from multiband transport. From the two-band analysis, we obtain the temperature-dependent carrier density and mobility of each band, as shown in Figs. 5(c)–5(f). In both compounds above 70 K, a single hole band dominates in transport with weakly temperature-dependent carrier density and mobility. Below 70 K, an electron band with a lower concentration but higher mobility comes into play. Still, holelike carriers dominate at low temperatures, in agreement with the positive Seebeck signal seen all the way from room temperature to 2 K [see Fig. 3(b)]. As shown in Figs. 1(c) and 1(d), the hole pockets around the zone boundary are mainly

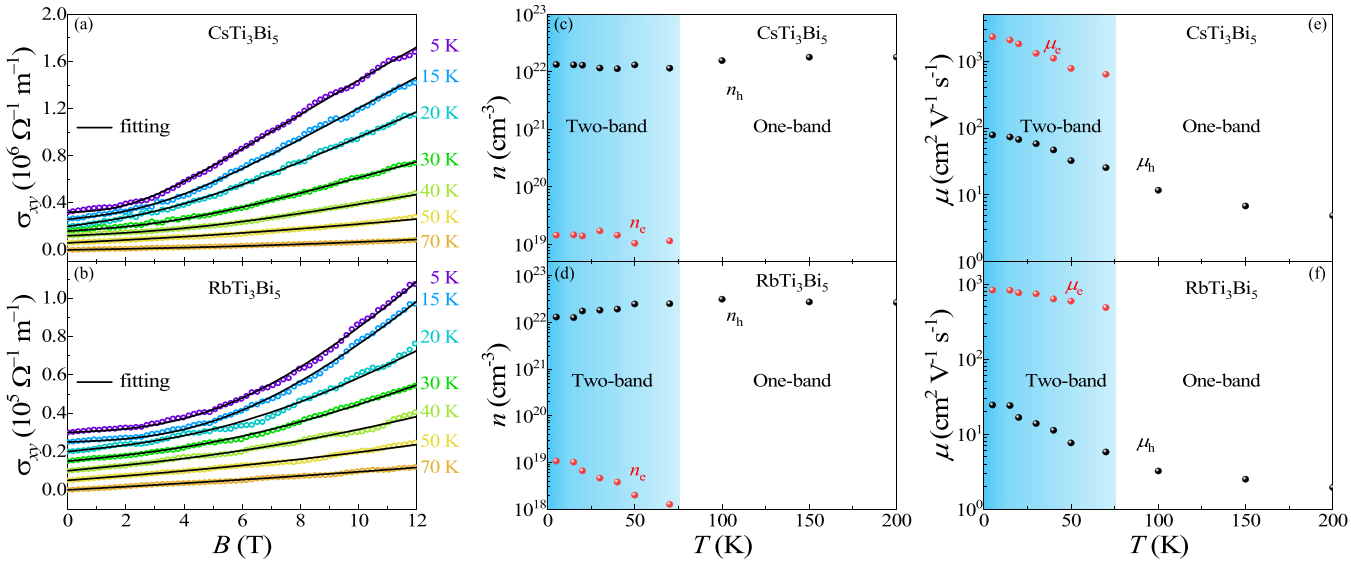

FIG. 5. (a) and (b) Electrical Hall conductivity (σ_{xy}) of $CsTi_3Bi_5$ and $RbTi_3Bi_5$. Scattered circular points are experimental data. Solid lines are theoretical fittings using a two-band model. Vertical offsets have been applied for clarity. (c)–(f) Temperature dependence of carrier density and mobility of each band obtained from the Hall conductivity.

contributed from Bi *d* orbitals. Therefore, the transport properties of ATi_3Bi_5 are dominated by Bi *d* orbitals. Similarly in AV_3Sb_5, the V *d* orbitals play dominant roles in transport properties and the formation of CDW [16,72]. In AV_3Sb_5, multiband transport effects also appear at low temperatures below about 50 K [28,29]. The multiband electronic structures thus play important roles in the transport behaviors of ATi_3Bi_5 and AV_3Sb_5, despite their different ground states. These results suggest that, in nonmagnetic multiband metals, an S-shaped nonlinear Hall response may not necessarily originate from an anomalous Hall effect, and contributions from multiband transport cannot be neglected.

IV. CONCLUSIONS

We have studied the electrical and thermal transport behaviors of the kagome metals ATi_3Bi_5. The structurally similar ATi_3Bi_5 and AV_3Sb_5 families share a few similarities but differ significantly. Both ATi_3Bi_5 and AV_3Sb_5 systems host multiband electronic structures, which are manifested in the nonlinear magnetic-field-dependent Hall effect at low temperatures. Unlike AV_3Sb_5, van Hove singularities in ATi_3Bi_5 are away from the Fermi level. In addition, the heat conduction in ATi_3Bi_5 is mainly carried by charge carriers, which is different from AV_3Sb_5 in which phonons and electron-phonon coupling contribute significantly. These differences between ATi_3Bi_5 and AV_3Sb_5 can provide important insights on the driving force of CDW in AV_3Sb_5.

ACKNOWLEDGMENTS

This work has been supported by National Natural Science Foundation of China (Grants No. 11904040, No. 52125103, No. 52071041, No. 12004254, No. 12004056, No. 11674384, and No. 11974065), Chinesisch-Deutsche Mobilitätsprogamm of Chinesisch-Deutsche Zentrum für Wissenschaftsförderung (Grant No. M-0496), and Chongqing Research Program of Basic Research and Frontier Technology, China (Grant No. cstc2020jcyj-msxmX0263). Y. Guo acknowledges the support by the Major Research Plan of the National Natural Science Foundation of China (No. 92065201), and the Double First-Class Initiative Fund of ShanghaiTech University. J. Shen acknowledges the support by National Natural Science Foundation of China (No. 12104254), and The Fundamental and Applied Fundamental Research Grant of Guangdong Province (No. 2021B1515120015). We thank the Hefei advanced computing center for technical support on theoretical calculations.

[1] I. Syôzi, Prog. Theor. Phys. **6**, 306 (1951).
[2] T. Neupert, M. M. Denner, J.-X. Yin, R. Thomale, and M. Z. Hasan, Nat. Phys. **18**, 137 (2022).
[3] A. O'Brien, F. Pollmann, and P. Fulde, Phys. Rev. B **81**, 235115 (2010).
[4] W.-H. Ko, P. A. Lee, and X.-G. Wen, Phys. Rev. B **79**, 214502 (2009).
[5] L. Balents, Nature (London) **464**, 199 (2010).
[6] M. L. Kiesel and R. Thomale, Phys. Rev. B **86**, 121105(R) (2012).
[7] M. L. Kiesel, C. Platt, and R. Thomale, Phys. Rev. Lett. **110**, 126405 (2013).
[8] S.-L. Yu and J.-X. Li, Phys. Rev. B **85**, 144402 (2012).
[9] B. R. Ortiz, L. C. Gomes, J. R. Morey, M. Winiarski, M. Bordelon, J. S. Mangum, I. W. H. Oswald, J. A. Rodriguez-Rivera, J. R. Neilson, S. D. Wilson, E. Ertekin, T. M.

McQueen, and E. S. Toberer, Phys. Rev. Mater. **3**, 094407 (2019).
[10] B. R. Ortiz, S. M. L. Teicher, Y. Hu, J. L. Zuo, P. M. Sarte, E. C. Schueller, A. M. Milinda Abeykoon, M. J. Krogstad, S. Rosenkranz, R. Osborn, R. Seshadri, L. Balents, J. He, and S. D. Wilson, Phys. Rev. Lett. **125**, 247002 (2020).
[11] B. R. Ortiz, P. M. Sarte, E. M. Kenney, M. J. Graf, S. M. L. Teicher, R. Seshadri, and S. D. Wilson, Phys. Rev. Mater. **5**, 034801 (2021).
[12] Q. Yin, Z. Tu, C. Gong, Y. Fu, S. Yan, and H. Lei, Chin. Phys. Lett. **38**, 037403 (2021).
[13] H. Li, T. T. Zhang, T. Yilmaz, Y. Y. Pai, C. E. Marvinney, A. Said, Q. W. Yin, C. S. Gong, Z. J. Tu, E. Vescovo, C. S. Nelson, R. G. Moore, S. Murakami, H. C. Lei, H. N. Lee, B. J. Lawrie, and H. Miao, Phys. Rev. X **11**, 031050 (2021).
[14] K. Nakayama, Y. Li, T. Kato, M. Liu, Z. Wang, T. Takahashi, Y. Yao, and T. Sato, Phys. Rev. B **104**, L161112 (2021).
[15] Z. Liu, N. Zhao, Q. Yin, C. Gong, Z. Tu, M. Li, W. Song, Z. Liu, D. Shen, Y. Huang, K. Liu, H. Lei, and S. Wang, Phys. Rev. X **11**, 041010 (2021).
[16] B. R. Ortiz, S. M. L. Teicher, L. Kautzsch, P. M. Sarte, N. Ratcliff, J. Harter, J. P. C. Ruff, R. Seshadri, and S. D. Wilson, Phys. Rev. X **11**, 041030 (2021).
[17] Y. Hu, S. M. Teicher, B. R. Ortiz, Y. Luo, S. Peng, L. Huai, J. Ma, N. C. Plumb, S. D. Wilson, J. He, and M. Shi, Sci. Bull. **67**, 495 (2022).
[18] Y. X. Jiang, J. X. Yin, M. M. Denner, N. Shumiya, B. R. Ortiz, G. Xu, Z. Guguchia, J. He, M. S. Hossain, X. Liu, J. Ruff, L. Kautzsch, S. S. Zhang, G. Chang, I. Belopolski, Q. Zhang, T. A. Cochran, D. Multer, M. Litskevich, Z. J. Cheng *et al.*, Nat. Mater. **20**, 1353 (2021).
[19] Z. Wang, Y.-X. Jiang, J.-X. Yin, Y. Li, G.-Y. Wang, H.-L. Huang, S. Shao, J. Liu, P. Zhu, N. Shumiya, M. S. Hossain, H. Liu, Y. Shi, J. Duan, X. Li, G. Chang, P. Dai, Z. Ye, G. Xu, Y. Wang *et al.*, Phys. Rev. B **104**, 075148 (2021).
[20] N. Shumiya, M. S. Hossain, J.-X. Yin, Y.-X. Jiang, B. R. Ortiz, H. Liu, Y. Shi, Q. Yin, H. Lei, S. S. Zhang, G. Chang, Q. Zhang, T. A. Cochran, D. Multer, M. Litskevich, Z.-J. Cheng, X. P. Yang, Z. Guguchia, S. D. Wilson, and M. Z. Hasan, Phys. Rev. B **104**, 035131 (2021).
[21] S.-Y. Yang, Y. Wang, B. R. Ortiz, D. Liu, J. Gayles, E. Derunova, R. Gonzalez-Hernandez, L. Šmejkal, Y. Chen, S. S. P. Parkin, S. D. Wilson, E. S. Toberer, T. McQueen, and M. N. Ali, Sci. Adv. **6**, eabb6003 (2020).
[22] F. H. Yu, T. Wu, Z. Y. Wang, B. Lei, W. Z. Zhuo, J. J. Ying, and X. H. Chen, Phys. Rev. B **104**, L041103 (2021).
[23] G. Zheng, C. Tan, Z. Chen, M. Wang, X. Zhu, S. Albarakati, M. Algarni, J. Partridge, L. Farrar, J. Zhou *et al.*, Nat. Commun. **14**, 678 (2023).
[24] D. Chen, B. He, M. Yao, Y. Pan, H. Lin, W. Schnelle, Y. Sun, J. Gooth, L. Taillefer, and C. Felser, Phys. Rev. B **105**, L201109 (2022).
[25] X. Zhou, H. Liu, W. Wu, K. Jiang, Y. Shi, Z. Li, Y. Sui, J. Hu, and J. Luo, Phys. Rev. B **105**, 205104 (2022).
[26] C. Mielke III, D. Das, J.-X. Yin, H. Liu, R. Gupta, Y.-X. Jiang, M. Medarde, X. Wu, H. C. Lei, J. Chang, P. Dai, Q. Si, H. Miao, R. Thomale, T. Neupert, Y. Shi, R. Khasanov, M. Z. Hasan, H. Luetkens, and Z. Guguchia, Nature (London) **602**, 245 (2022).
[27] L. Yu, C. Wang, Y. Zhang, M. Sander, S. Ni, Z. Lu, S. Ma, Z. Wang, Z. Zhao, H. Chen, K. Jiang, Y. Zhang, H. Yang, F. Zhou, X. Dong, S. L. Johnson, M. J. Graf, J. Hu, H.-J. Gao, and Z. Zhao, arXiv:2107.10714.
[28] Y. Gan, W. Xia, L. Zhang, K. Yang, X. Mi, A. Wang, Y. Chai, Y. Guo, X. Zhou, and M. He, Phys. Rev. B **104**, L180508 (2021).
[29] X. Mi, W. Xia, L. Zhang, Y. Gan, K. Yang, A. Wang, Y. Chai, Y. Guo, X. Zhou, and M. He, New J. Phys. **24**, 093021 (2022).
[30] Z. Liang, X. Hou, F. Zhang, W. Ma, P. Wu, Z. Zhang, F. Yu, J.-J. Ying, K. Jiang, L. Shan, Z. Wang, and X.-H. Chen, Phys. Rev. X **11**, 031026 (2021).
[31] H. Zhao, H. Li, B. R. Ortiz, S. M. L. Teicher, T. Park, M. Ye, Z. Wang, L. Balents, S. D. Wilson, and I. Zeljkovic, Nature (London) **599**, 216 (2021).
[32] H. Chen, H. Yang, B. Hu, Z. Zhao, J. Yuan, Y. Xing, G. Qian, Z. Huang, G. Li, Y. Ye, S. Ma, S. Ni, H. Zhang, Q. Yin, C. Gong, Z. Tu, H. Lei, H. Tan, S. Zhou, C. Shen *et al.*, Nature (London) **599**, 222 (2021).
[33] H.-S. Xu, Y.-J. Yan, R. Yin, W. Xia, S. Fang, Z. Chen, Y. Li, W. Yang, Y. Guo, and D.-L. Feng, Phys. Rev. Lett. **127**, 187004 (2021).
[34] H. Li, H. Zhao, B. R. Ortiz, T. Park, M. Ye, L. Balents, Z. Wang, S. D. Wilson, and I. Zeljkovic, Nat. Phys. **18**, 265 (2022).
[35] Y. Hu, X. Wu, B. R. Ortiz, X. Han, N. C. Plumb, S. D. Wilson, A. P. Schnyder, and M. Shi, Phys. Rev. B **106**, L241106 (2022).
[36] F. H. Yu, D. H. Ma, W. Z. Zhuo, S. Q. Liu, X. K. Wen, B. Lei, J. J. Ying, and X. H. Chen, Nat. Commun. **12**, 3645 (2021).
[37] F. Yu, X. Zhu, X. Wen, Z. Gui, Z. Li, Y. Han, T. Wu, Z. Wang, Z. Xiang, Z. Qiao, J. Ying, and X. Chen, Phys. Rev. Lett. **128**, 077001 (2022).
[38] Z. Zhang, Z. Chen, Y. Zhou, Y. Yuan, S. Wang, J. Wang, H. Yang, C. An, L. Zhang, X. Zhu, Y. Zhou, X. Chen, J. Zhou, and Z. Yang, Phys. Rev. B **103**, 224513 (2021).
[39] F. Du, S. Luo, B. R. Ortiz, Y. Chen, W. Duan, D. Zhang, X. Lu, S. D. Wilson, Y. Song, and H. Yuan, Phys. Rev. B **103**, L220504 (2021).
[40] F. Du, R. Li, S. Luo, Y. Gong, Y. Li, S. Jiang, B. R. Ortiz, Y. Liu, X. Xu, S. D. Wilson, C. Cao, Y. Song, and H. Yuan, Phys. Rev. B **106**, 024516 (2022).
[41] C. C. Zhu, X. F. Yang, W. Xia, Q. W. Yin, L. S. Wang, C. C. Zhao, D. Z. Dai, C. P. Tu, B. Q. Song, Z. C. Tao, Z. J. Tu, C. S. Gong, H. C. Lei, Y. F. Guo, and S. Y. Li, Phys. Rev. B **105**, 094507 (2022).
[42] X. Chen, X. Zhan, X. Wang, J. Deng, X.-B. Liu, X. Chen, J.-G. Guo, and X. Chen, Chin. Phys. Lett. **38**, 057402 (2021).
[43] K. Y. Chen, N. N. Wang, Q. W. Yin, Y. H. Gu, K. Jiang, Z. J. Tu, C. S. Gong, Y. Uwatoko, J. P. Sun, H. C. Lei, J. P. Hu, and J.-G. Cheng, Phys. Rev. Lett. **126**, 247001 (2021).
[44] N. N. Wang, K. Y. Chen, Q. W. Yin, Y. N. N. Ma, B. Y. Pan, X. Yang, X. Y. Ji, S. L. Wu, P. F. Shan, S. X. Xu, Z. J. Tu, C. S. Gong, G. T. Liu, G. Li, Y. Uwatoko, X. L. Dong, H. C. Lei, J. P. Sun, and J.-G. Cheng, Phys. Rev. Res. **3**, 043018 (2021).
[45] Y. M. Oey, B. R. Ortiz, F. Kaboudvand, J. Frassineti, E. Garcia, R. Cong, S. Sanna, V. F. Mitrović, R. Seshadri, and S. D. Wilson, Phys. Rev. Mater. **6**, L041801 (2022).
[46] H. Yang, Z. Huang, Y. Zhang, Z. Zhao, J. Shi, H. Luo, L. Zhao, G. Qian, H. Tan, B. Hu, K. Zhu, Z. Lu, H. Zhang, J. Sun, J. Cheng, C. Shen, X. Lin, B. Yan, X. Zhou, Z. Wang *et al.*, Sci. Bull. **67**, 2176 (2022).

[47] M. Shi, F. Yu, Y. Yang, F. Meng, B. Lei, Y. Luo, Z. Sun, J. He, R. Wang, Z. Jiang, Z. Liu, D. Shen, T. Wu, Z. Wang, Z. Xiang, J. Ying, and X. Chen, Nat. Commun. **13**, 2773 (2022).
[48] Q. Yin, Z. Tu, C. Gong, S. Tian, and H. Lei, Chin. Phys. Lett. **38**, 127401 (2021).
[49] N. Wang, Y. Gu, M. A. McGuire, J. Yan, L. Shi, Q. Cui, K. Chen, Y. Wang, H. Zhang, H. Yang, X. Dong, K. Jiang, J. Hu, B. Wang, J. Sun, and J. Cheng, Chin. Phys. B **31**, 017106 (2022).
[50] Y. Yang, W. Fan, Q. Zhang, Z. Chen, X. Chen, T. Ying, X. Wu, X. Yang, F. Meng, G. Li, S. Li, L. Gu, T. Qian, A. P. Schnyder, J.-g. Guo, and X. Chen, Chin. Phys. Lett. **38**, 127102 (2021).
[51] S. Peng, Y. Han, G. Pokharel, J. Shen, Z. Li, M. Hashimoto, D. Lu, B. R. Ortiz, Y. Luo, H. Li, M. Guo, B. Wang, S. Cui, Z. Sun, Z. Qiao, S. D. Wilson, and J. He, Phys. Rev. Lett. **127**, 266401 (2021).
[52] Y. Hu, X. Wu, Y. Yang, S. Gao, N. C. Plumb, A. P. Schnyder, W. Xie, J. Ma, and M. Shi, Sci. Adv. **8**, eadd2024 (2022).
[53] X.-W. Yi, X.-Y. Ma, Z. Zhang, Z.-W. Liao, J.-Y. You, and G. Su, Phys. Rev. B **106**, L220505 (2022).
[54] Y. Jiang, Z. Yu, Y. Wang, T. Lu, S. Meng, K. Jiang, and M. Liu, Chin. Phys. Lett. **39**, 047402 (2022).
[55] D. Werhahn, B. R. Ortiz, A. K. Hay, S. D. Wilson, R. Seshadri, and D. Johrendt, Z. Naturforsch. B **77**, 757 (2022).
[56] H. Yang, Z. Zhao, X.-W. Yi, J. Liu, J.-Y. You, Y. Zhang, H. Guo, X. Lin, C. Shen, H. Chen, X. Dong, G. Su, and H.-J. Gao, arXiv:2209.03840.
[57] H. Yang, Y. Ye, Z. Zhao, J. Liu, X.-W. Yi, Y. Zhang, J. Shi, J.-Y. You, Z. Huang, B. Wang, J. Wang, H. Guo, X. Lin, C. Shen, W. Zhou, H. Chen, X. Dong, G. Su, Z. Wang, and H.-J. Gao, arXiv:2211.12264.
[58] Y. Hu, C. Le, Z. Zhao, J. Ma, N. C. Plumb, M. Radovic, A. P. Schnyder, X. Wu, H. Chen, X. Dong, J. Hu, H. Yang, H.-J. Gao, and M. Shi, arXiv:2212.07958.
[59] Z. Jiang, Z. Liu, H. Ma, W. Xia, Z. Liu, J. Liu, S. Cho, Y. Yang, J. Ding, J. Liu, Z. Huang, Y. Qiao, J. Shen, W. Jing, X. Liu, J. Liu, Y. Guo, and D. Shen, arXiv:2212.02399.
[60] Y. Zhou, L. Chen, X. Ji, C. Liu, K. Liao, Z. Guo, J. Wang, H. Weng, and G. Wang, arXiv:2301.01633.
[61] W. Kohn and L. J. Sham, Phys. Rev. **140**, A1133 (1965).
[62] G. Kresse and J. Furthmüller, Phys. Rev. B **54**, 11169 (1996).
[63] G. Kresse and J. Furthmüller, Comput. Mater. Sci. **6**, 15 (1996).
[64] P. E. Blöchl, Phys. Rev. B **50**, 17953 (1994).
[65] G. Kresse and D. Joubert, Phys. Rev. B **59**, 1758 (1999).
[66] J. P. Perdew, K. Burke, and M. Ernzerhof, Phys. Rev. Lett. **77**, 3865 (1996).
[67] M. Kang, S. Fang, J.-K. Kim, B. R. Ortiz, S. H. Ryu, J. Kim, J. Yoo, G. Sangiovanni, D. D. Sante, B.-G. Park, C. Jozwiak, A. Bostwick, E. Rotenberg, E. Kaxiras, S. D. Wilson, J.-H. Park, and R. Comin, Nat. Phys. **18**, 301 (2022).
[68] X. Zhou, Y. Li, X. Fan, J. Hao, Y. Dai, Z. Wang, Y. Yao, and H.-H. Wen, Phys. Rev. B **104**, L041101 (2021).
[69] Y. Hu, X. Wu, B. R. Ortiz, S. Ju, X. Han, J. Ma, N. C. Plumb, M. Radovic, R. Thomale, S. D. Wilson, A. P. Schnyder, and M. Shi, Nat. Commun. **13**, 2220 (2022).
[70] B. W. Roberts, J. Phys. Chem. Ref. Data **5**, 581 (1976).
[71] K. Yang, W. Xia, X. Mi, L. Zhang, Y. Gan, A. Wang, Y. Chai, X. Zhou, X. Yang, Y. Guo, and M. He, arXiv:2211.04216.
[72] K. Jiang, T. Wu, J.-X. Yin, Z. Wang, M. Z. Hasan, S. D. Wilson, X. Chen, and J. Hu, Natl. Sci. Rev. **10**, nwac199 (2023).